J|A|C|S ARTICLES

Published on Web 02/26/2010

Carbamate Transport in Carbamoyl Phosphate Synthetase: A Theoretical and Experimental Investigation

Liliya Lund, Yubo Fan, Qiang Shao, Yi Qin Gao,* and Frank M. Raushel*

Department of Chemistry, Texas A&M University, College Station, Texas 77843-3255

Received December 10, 2009; E-mail: yiqin@mail.chem.tamu.edu; raushel@tamu.edu

Abstract: The transport of carbamate through the large subunit of carbamoyl phosphate synthetase (CPS) from *Escherichia coli* was investigated by molecular dynamics and site-directed mutagenesis. Carbamate, the product of the reaction involving ATP, bicarbonate, and ammonia, must be delivered from the site of formation to the site of utilization by traveling nearly 40 Å within the enzyme. Potentials of mean force (PMF) calculations along the entire tunnel for the translocation of carbamate indicate that the tunnel is composed of three continuous water pockets and two narrow connecting parts, near Ala-23 and Gly-575. The two narrow parts render two free energy barriers of 6.7 and 8.4 kcal/mol, respectively. Three water pockets were filled with about 21, 9, and 9 waters, respectively, and the corresponding relative free energies of carbamate residing in these free energy minima are 5.8, 0, and 1.6 kcal/mol, respectively. The release of phosphate into solution at the site for the formation of carbamate allows the side chain of Arg-306 to rotate toward Glu-25, Glu-383, and Glu-604. This rotation is virtually prohibited by a barrier of at least 23 kcal/mol when phosphate remains bound. This conformational change not only opens the entrance of the tunnel but also shields the charge−charge repulsion from the three glutamate residues when carbamate passes through the tunnel. Two mutants, A23F and G575F, were designed to block the migration of carbamate through the narrowest parts of the carbamate tunnel. The mutants retained only 1.7% and 3.8% of the catalytic activity for the synthesis of carbamoyl phosphate relative to the wild type CPS, respectively.

Introduction

Carbamoyl phosphate synthetase (CPS) from *Escherichia coli* catalyzes the formation of carbamoyl phosphate, an intermediate in the biosynthesis of pyrimidine nucleotides and arginine, from glutamine, bicarbonate, and two molecules of MgATP.[1−3] In the proposed reaction mechanism, ATP phosphorylates bicarbonate to form carboxy phosphate, and glutamine is hydrolyzed to glutamate and ammonia. The ammonia then reacts with the carboxy phosphate intermediate to form carbamate. In the final step, a second molecule of ATP phosphorylates carbamate to produce the ultimate product, carbamoyl phosphate. Overall, three unstable intermediates (ammonia, carboxy phosphate, and carbamate) and carbamoyl phosphate are formed in a series of four separate reactions. The reaction mechanism is summarized in Scheme 1.

CPS from *E. coli* is a heterodimeric protein that is composed of two subunits of molecular weight ∼40 and ∼118 kD.[4] The hydrolysis of glutamine occurs within the small subunit, whereas carbamoyl phosphate is produced in the large subunit.[5] The catalytic properties of site-directed mutants and the X-ray structure of CPS have identified the N-terminal half of the large subunit as containing the active site for the formation of carboxy phosphate and carbamate, whereas the C-terminal half harbors

Scheme 1

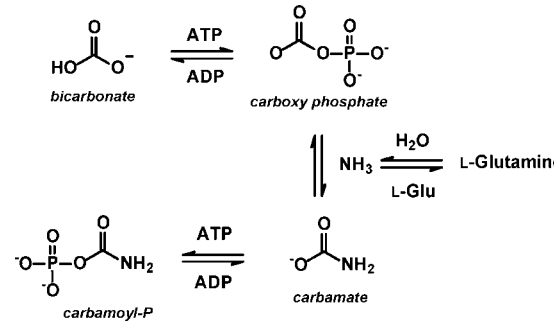

the active site for the synthesis of carbamoyl phosphate. The three active sites are connected by two molecular tunnels that extend nearly 100 Å from one end of the protein to the other as illustrated in Figure 1.[6] Ammonia migrates from the site of synthesis in the small subunit to the site of utilization in the N-terminal domain of the large subunit through a passageway designated as the "ammonia tunnel". After carbamate is formed from the reaction of ammonia with carboxy phosphate, this intermediate migrates through the "carbamate tunnel" to the third active site where it is phosphorylated by the second ATP to carbamoyl phosphate. Of the thirty residues that come together to form the carbamate tunnel, half come from the N-terminal domain, with the remaining half coming from the C-terminal domain. The tunnel is capped at both ends by arginine residues,

(1) Pierard, A.; Wiame, J. M. *Biochem. Biophys. Res. Commun.* **1964**, *15*, 76–81.
(2) Anderson, P. M.; Meister, A. *Biochemistry* **1966**, *5*, 3164–3169.
(3) Anderson, P. M. *Biochemistry* **1977**, *16*, 587–593.
(4) Matthews, S. L.; Anderson, P. M. *Biochemistry* **1972**, *11*, 1176–1183.
(5) Trotta, P. P.; Burt, M. E.; Haschemeyer, R. H.; Meister, A. *Proc. Natl. Acad. Sci. U.S.A.* **1971**, *68*, 2599–2603.
(6) Thoden, J. B.; Holden, H. M.; Wesenberg, G.; Raushel, F. M.; Rayment, I. *Biochemistry* **1997**, *36*, 6305–6316.

10.1021/ja910441v

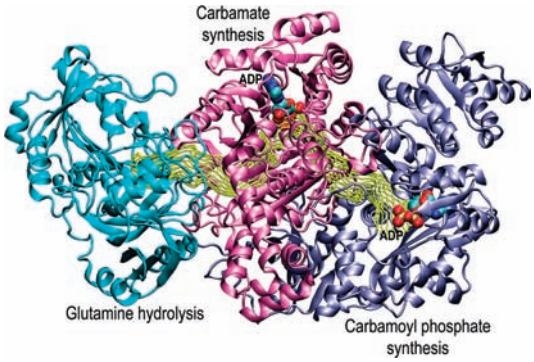

Figure 1. Structure of carbamoyl phosphate synthetase. The small subunit that contains the active site for the hydrolysis of glutamine is shown in green. The N-terminal domain of the large subunit that contains the active site for the synthesis of carboxy phosphate and carbamate is shown in red. The C-terminal domain of the large subunit that contains the active site for the synthesis of carbamoyl phosphate is shown in blue. The two molecular tunnels for the translocation of ammonia and carbamate are shown in yellow dotted lines. The image was constructed from PDB file: 1C30.

Arg-306 from the N-terminal domain and Arg-848 from the C-terminal domain. While the tunnel itself is comprised primarily of nonionic amino acids, five glutamate residues, Glu-25, Glu-383, Glu-604, Glu-577, and Glu-916 are positioned with their side chains pointing to the interior of the carbamate tunnel. These residues are highly conserved in CPS from both eukaryotic and prokaryotic species.

Enzymes have evolved molecular tunnels to protect unstable and reactive intermediates from bulk solvent. Protein tunnels for the migration of ammonia have been found in all members of the glutamine amidotransferase family of enzymes.[6−16] In addition to the transport of ammonia, tunnels have been identified for the translocation of other reactive species. For example, tryptophan synthase,[17−19] acetyl-coenzyme A synthase/carbon monoxide dehydrogenase,[20−22] 4-hydroxy-2-ketovalerate aldolase /acylating acetaldehyde dehydrogenase,[23] and CPS use molecular tunnels to transport indole, carbon monoxide, acetaldehyde, and carbamate, respectively.

Molecular dynamics (MD) simulations have proven useful in the functional analysis of tunnels in enzyme catalyzed reactions. This technique has facilitated the elucidation of the mechanism for the migration of reaction intermediates at the atomic level and has yielded insights on the thermodynamics, kinetics, and dynamics of these processes. MD simulations on ammonia tunneling have provided a better understanding of the transport path for ammonia and the interactions of this intermediate with the protein environment. For example, the transfer of NH_3 in imidazole glycerol phosphate synthase and glucosamine-6-phosphate synthase was studied using steered MD.[24−26] In addition, the free energy profile for NH_3 transport in AmtB was calculated using an umbrella sampling technique,[27] and it was also investigated with conventional MD simulations.[28] More recently, we have reported on the mechanism for the translocation of ammonia in CPS using MD simulations.[29,30] Our calculations identified the rate-determining step for ammonia transport with a free energy barrier of 7.2 kcal/mol as it passed through a narrow turning gate surrounded by the side chains of Cys-232, Ala-251, and Ala-314 in the large subunit. Complete blockage of this passageway was achieved by construction of a mutant, C232V/A251V/A314V, which was unable to synthesize carbamoyl phosphate using glutamine as a nitrogen source.

In this paper, we have calculated the free energy profile for the migration of carbamate along the carbamate tunnel using the umbrella sampling technique. The transport of carbamate through the entire carbamate tunnel is composed of three steps. The sequence of events is initiated by the reaction of ammonia with carboxy phosphate to form carbamate and phosphate. Phosphate is released into solution and the side chain of Arg-306 rotates toward the interior of the carbamate tunnel and locked in place by electrostatic interactions with Glu-25, Glu-383, and Glu-604 before carbamate is injected into the tunnel. After passing through a relatively narrow region surrounded by Ile-18, Ile-20, Ala-23, and Val-381 with a free energy barrier of 6.7 kcal/mol, carbamate enters a large water pocket in the middle of the tunnel with a free energy drop of 12 kcal/mol. Carbamate approaches the site of phosphorylation in the C-terminal domain of the large subunit by overcoming a free energy barrier of 8.4 kcal/mol near the juxtaposition Glu-577, Glu-916, and Arg-848. In this simulation, carbamate travels nearly 30 Å through the internal water-tight tunnel from the

(7) Krahn, J. M.; Kim, J. H.; Burns, M. R.; Parry, R. J.; Zalkin, H.; Smith, J. L. *Biochemistry* **1997**, *36*, 11061–11068.
(8) Larsen, T. M.; Boehlein, S. K.; Schuster, S. M.; Richards, N. G. J.; Thoden, J. B.; Holden, H. M.; Rayment, I. *Biochemistry* **1999**, *38*, 16146–16157.
(9) van den Heuvel, R. H. H.; Ferrari, D.; Bossi, R. T.; Ravasio, S.; Curti, B.; Vanoni, M. A.; Florencio, F. J.; Mattevi, A. *J. Biol. Chem.* **2002**, *277*, 24579–24583.
(10) Douangamath, A.; Walker, M.; Beismann-Driemeyer, S.; Vega-Fernandez, M. C.; Sterner, R.; Wilmanns, M. *Structure* **2002**, *10*, 185–193.
(11) Mouilleron, S.; Badet-Denisot, M. A.; Golinelli-Pimpaneau, B. *J. Biol. Chem.* **2006**, *281*, 4404–4412.
(12) Teplyakov, A.; Obmolova, G.; Badet, B.; Badet-Denisot, M. A. *J. Mol. Biol.* **2001**, *313*, 1093–1102.
(13) Schmitt, E.; Panvert, M.; Blanquet, S.; Mechulam, Y. *Structure* **2005**, *13*, 1421–1433.
(14) LaRonde-LeBlanc, N.; Resto, M.; Gerratana, B. *Nat. Struct. Mol. Biol.* **2009**, *16*, 421–429.
(15) Wojcik, M.; Seidle, H. F.; Bieganowski, P.; Brenner, C. *J. Biol. Chem.* **2006**, *281*, 33395–33402.
(16) Raushel, F. M.; Thoden, J. B.; Holden, H. M. *Acc. Chem. Res.* **2003**, *36*, 539–548.
(17) Hyde, C. C.; Ahmed, S. A.; Padlan, E. A.; Miles, E. W.; Davies, D. R. *J. Biol. Chem.* **1988**, *263*, 17857–17871.
(18) Barends, T. R. M.; Dunn, M. F.; Schlichting, I. *Curr. Opin. Chem. Biol.* **2008**, *12*, 593–600.
(19) Dunn, M. F.; Niks, D.; Ngo, H.; Barends, T. R. M.; Schlichting, I. *Trends Biochem. Sci.* **2008**, *33*, 254–264.
(20) Tan, X. S.; Volbeda, A.; Fontecilla-Camps, J. C.; Lindahl, P. A. *J. Biol. Inorg. Chem.* **2006**, *11*, 371–378.
(21) Tan, X. S.; Loke, H. K.; Fitch, S.; Lindahl, P. A. *J. Am. Chem. Soc.* **2005**, *127*, 5833–5839.
(22) Maynard, E. L.; Lindahl, P. A. *Biochemistry* **2001**, *40*, 13262–13267.
(23) Manjasetty, B. A.; Powlowski, J.; Vrielink, A. *Proc. Natl. Acad. Sci. U. S. A.* **2003**, *100*, 6992–6997.
(24) Amaro, R.; Luthey-Schulten, Z. *Chem. Phys.* **2004**, *307*, 147–155.
(25) Amaro, R. E.; Myers, R. S.; Davisson, V. J.; Luthey-Schulten, Z. A. *Biophys. J.* **2005**, *89*, 475–487.
(26) Floquet, N.; Mouilleron, S.; Daher, R.; Maigret, B.; Badet, B.; Badet-Denisot, M. A. *FEBS Lett.* **2007**, *581*, 2981–2987.
(27) Lin, Y. C.; Cao, Z. X.; Mo, Y. R. *J. Am. Chem. Soc.* **2006**, *128*, 10876–10884.
(28) Yang, H. Y.; Xu, Y. C.; Zhu, W. L.; Chen, K. X.; Jiang, H. L. *Biophys. J.* **2007**, *92*, 877–885.
(29) Fan, Y. B.; Lund, L.; Shao, Q.; Gao, Y. Q.; Raushel, F. M. *J. Am. Chem. Soc.* **2009**, *131*, 10211–10219.
(30) Fan, Y. B.; Lund, L.; Yang, L. J.; Raushel, F. M.; Gao, Y. Q. *Biochemistry* **2008**, *47*, 2935–2944.

Table 1. Definition of the Complexes with Different Ligands Bound

		substrate(s)		
name	PDB code	site 1[a]	site 2[b]	Arg-306[c]
A	1bxr	ADP	ATP	open
B	1bxr	ADP + P_i	ATP	closed
C	1c30	ADP + P_i	ADP	open

[a] Site for carbamate synthesis. [b] Site for carbamoyl phosphate synthesis. [c] When Arg-306 is hydrogen bonded to the phosphate site 1 the tunnel is closed and it is open when this residue is hydrogen bonded to Glu-25, Glu-383, and Glu-604.

site of formation in the N-terminal domain to the site of utilization in the C-terminal domain of CPS.

Materials and Methods

Construction of Models for the Transport of Carbamate. The large subunit from the X-ray crystal structure of CPS (PDB codes: 1c30 and 1bxr) was taken as the starting point for the simulations of carbamate transfer in CPS.[31,32] In one of these structures (PDB code: 1c30) ADP and phosphate are bound in the active site for carbamate formation whereas ADP alone is bound in the active site for the synthesis of carbamoyl phosphate. In the other structure (PDB code: 1bxr) AMPPNP, an ATP analogue, is bound to both active sites in the large subunit of CPS. Two missing loops (residues 717−723 and 742−749) in the large subunit of CPS (PDB code: 1c30) were inserted using SWISS-MODEL.[33−35] These two loops are part of the binding site for ATP in the carbamoyl phosphate synthesis domain. Without the γ-phosphate of the substrate, the domain containing these two loops is apparently flexible. In the large subunit, obtained from the structure represented by PDB code 1bxr, the bound AMPPNP was substituted with ATP in the active site for the phosphorylation of carbamate. Conversely, in the active site for the phosphorylation of bicarbonate, AMPPNP was substituted with ADP and phosphate, or ADP alone. Three structural complexes were created for the simulations and these are denoted as complexes **A**, **B** and **C** in Table 1.

The charge distributions on all atoms in carbamate were obtained using the RESP-fit method[36,37] based on B3LYP/cc-pVTZ calculations[38−41] with the solvent effect ($\epsilon = 4$) taken into account using the polarizable continuum model (PCM).[42−44] Before charge fitting, the geometry for carbamate was fully optimized in the gas phase at the same theoretical level. The charges on the carbon, hydrogen, oxygen, and nitrogen atoms in carbamate are +0.883517, +0.325533, −0.824983, and −0.884618, respectively. Mn^{2+} and all of the crystalline waters within the enzyme or on the protein exterior were utilized for the simulations. The protonation states of all histidine residues were adjusted based on local environments. The net negative charge of the protein was neutralized by added Na^+ ions. Explicit TIP3P waters were added as a truncated octahedral water box with a 10 Å buffer.[45] All operations were processed using the AMBER Leap module, which led to models containing ~70 000 atoms, including ~19 000 waters.[46,47] These models were further extended using the periodic boundary condition. The AMBER force field 99,[48] with the parameters for the peptide backbone reoptimized, was utilized for all standard amino acid residues while the general AMBER force field was used for carbamate.[49] The force fields for ADP, P_i, and Mn^{2+} were previously developed for the Amber program.[50,51] MD simulations were conducted in an isothermal−isobaric (NPT) ensemble at 300 K and 1 atm. The SHAKE algorithm was used to constrain all bonds involving hydrogens.[52] A 10 Å cutoff was applied for nonbonding interactions. The Particle Mesh Ewald method was employed to treat long-range electrostatic interactions.[53,54]

MD trajectories were obtained with these structures using the AMBER suite of programs.[46,47] Before the MD simulations, in which the trajectories were collected every 0.5 ps, two steps of minimization were conducted. During minimization, the systems were first optimized for 1000 cycles while the backbone of the protein was frozen with a force constant of 500 kcal·mol^{-1}·Å^{-2}. The systems were further optimized for 2500 cycles without constraints, followed by a 20-ps MD simulation which heats the system from 0 to 300 K, with a force constant of 10 kcal·mol^{-1}·Å^{-2} added upon the protein backbone. A 200-ps simulation under 1 atm and 300 K was performed to reach equilibrium with the constraints on the protein removed.

Free Energy Calculations. The reaction coordinate for the free-energy simulations was defined as the distance from the carbon atom (C_{cbm}) of carbamate to the β-phosphoryl group of ADP in the active site for carbamate formation as shown in Figure 2. The free-energy profiles or potentials of mean force (PMF) were computed along the translocation trajectories using the umbrella sampling technique with a biasing harmonic potential involving a force constant of 40 kcal·mol^{-1}·Å^{-2}.[55−59] A total of 113 windows were chosen for each of the three systems with a step size of 0.25 Å starting from 5 Å and ending at 33 Å. An equilibration simulation for each window was performed and the corresponding PMF along the reaction coordinate was computed every 500 ps using the weighted histogram analysis method (WHAM)[56−58] until convergence was observed. The last four 500-ps trajectories, without yielding significantly different PMF when used separately, were combined as a 2-ns simulation for WHAM analysis. Because of

(31) Thoden, J. B.; Huang, X. Y.; Raushel, F. M.; Holden, H. M. *Biochemistry* **1999**, *38*, 16158–16166.
(32) Thoden, J. B.; Wesenberg, G.; Raushel, F. M.; Holden, H. M. *Biochemistry* **1999**, *38*, 2347–2357.
(33) Schwede, T.; Kopp, J.; Guex, N.; Peitsch, M. C. *Nucleic Acids Res.* **2003**, *31*, 3381–3385.
(34) Kopp, J.; Schwede, T. *Nucleic Acids Res.* **2004**, *32*, D230−D234.
(35) Arnold, K.; Bordoli, L.; Kopp, J.; Schwede, T. *Bioinformatics* **2006**, *22*, 195–201.
(36) Singh, U. C.; Kollman, P. A. *J. Comput. Chem.* **1984**, *5*, 129–145.
(37) Besler, B. H.; Merz, K. M.; Kollman, P. A. *J. Comput. Chem.* **1990**, *11*, 431–439.
(38) Becke, A. D. *Phys. Rev. A: At. Mol. Opt. Phys.* **1988**, *38*, 3098–3100.
(39) Lee, C. T.; Yang, W. T.; Parr, R. G. *Phys. Rev. B: Condens. Matter* **1988**, *37*, 785–789.
(40) Becke, A. D. *J. Chem. Phys.* **1993**, *98*, 1372–1377.
(41) Kendall, R. A.; Dunning, T. H.; Harrison, R. J. *J. Chem. Phys.* **1992**, *96*, 6796–6806.
(42) Cances, E.; Mennucci, B.; Tomasi, J. *J. Chem. Phys.* **1997**, *107*, 3032–3041.
(43) Cossi, M.; Barone, V.; Mennucci, B.; Tomasi, J. *Chem. Phys. Lett.* **1998**, *286*, 253–260.
(44) Mennucci, B.; Tomasi, J. *J. Chem. Phys.* **1997**, *106*, 5151–5158.
(45) Jorgensen, W. L.; Chandrasekhar, J.; Madura, J. D.; Impey, R. W.; Klein, M. L. *J. Chem. Phys.* **1983**, *79*, 926–935.
(46) Case, D. A.; et al. *AMBER 9*; University of California: San Francisco, 2006.
(47) Case, D. A.; et al. *AMBER 8*; University of California: San Francisco, 2004.
(48) Wang, J. M.; Cieplak, P.; Kollman, P. A. *J. Comput. Chem.* **2000**, *21*, 1049–1074.
(49) Wang, J. M.; Wolf, R. M.; Caldwell, J. W.; Kollman, P. A.; Case, D. A. *J. Comput. Chem.* **2004**, *25*, 1157–1174.
(50) Meagher, K. L.; Redman, L. T.; Carlson, H. A. *J. Comput. Chem.* **2003**, *24*, 1016–1025.
(51) Bradbrook, G. M.; Gleichmann, T.; Harrop, S. J.; Habash, J.; Raftery, J.; Kalb, J.; Yariv, J.; Hillier, I. H.; Helliwell, J. R. *J. Chem. Soc., Faraday Trans.* **1998**, *94*, 1603–1611.
(52) van Gunsteren, W. F.; Berendsen, H. J. C. *Mol. Phys.* **1977**, *34*, 1311–1327.
(53) Darden, T.; York, D.; Pedersen, L. *J. Chem. Phys.* **1993**, *98*, 10089–10092.
(54) Essmann, U.; Perera, L.; Berkowitz, M. L.; Darden, T.; Lee, H.; Pedersen, L. G. *J. Chem. Phys.* **1995**, *103*, 8577–8593.
(55) Kottalam, J.; Case, D. A. *J. Am. Chem. Soc.* **1988**, *110*, 7690–7697.
(56) Kumar, S.; Bouzida, D.; Swendsen, R. H.; Kollman, P. A.; Rosenberg, J. M. *J. Comput. Chem.* **1992**, *13*, 1011–1021.
(57) Kumar, S.; Rosenberg, J. M.; Bouzida, D.; Swendsen, R. H.; Kollman, P. A. *J. Comput. Chem.* **1995**, *16*, 1339–1350.
(58) Roux, B. *Comput. Phys. Commun.* **1995**, *91*, 275–282.
(59) Vallequ, J. P.; Torrie, G. M. *Statistical Mechanics, Part A, Equilibrium Techniques*; Plenum Press: New York, 1977; Vol. 5.

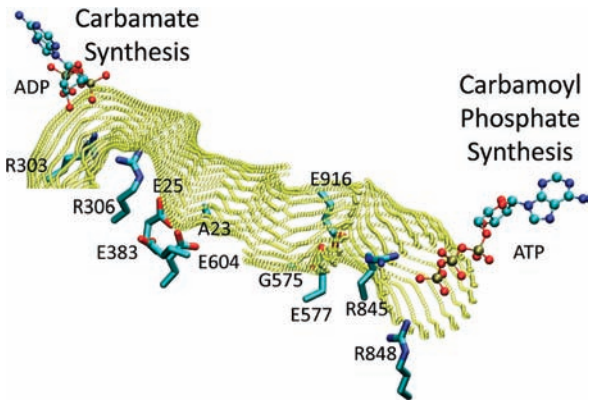

Figure 2. Molecular tunnel for the transport of carbamate from the site of its formation to the site of the carbamoyl phosphate synthesis. ADP and ATP are bound to the sites for carbamate formation and utilization, respectively. The transport of carbamate starts in the area near Arg-303 and Arg-306 and ends near Arg-845. There are two narrow regions of the tunnel near Ala-23 and Gly-575.

the repulsion between carbamate and phosphate in complexes **B** and **C** when the reaction coordinate is shorter than 10 Å, the PMFs for these two systems were calculated from 10 to 33 Å. Because of the complexity of the tunnel, the distances from C_{cbm} to C_{α} of Gly-575 and that from C_{cbm} to C_{β} of Ala-23, were defined to compute the PMFs for the first and second halves of the tunnel, respectively. The results further verified the validity of the PMF for the overall reaction coordinate mentioned above (see Figure S1).

Bacterial Strains and Plasmids. Site-directed mutagenesis of CPS was performed as described previously.[60,61] The *E. coli* strains used for this study were RC50 (*car*A50, *thi*−1, *mal*A1, *xyl*−7, *rsp*L135, *λ*r, *λ*-, and *tsx*−237) and XL1-Blue. The RC50 strain used for protein expression was a generous gift from Dr. Carol J. Lusty. All plasmids used in this project were derived from pMS03.[61] Oligonucleotide synthesis and DNA sequencing reactions were performed by the Gene Technology Laboratory, Texas A&M University. Site-directed mutagenesis was performed using the QuikChange protocol from Stratagene. All of the site-directed changes made to the wild-type CPS were confirmed by DNA sequencing of the modified plasmids.

Expression and Purification of Mutant Proteins. The plasmids containing the *car*AB genes were transformed in the RC50 cell line of *E. coli* for expression of the wild-type and mutant forms of CPS, and the proteins were purified as previously described.[62] The mutants A23F, A23K, M174M, M378E, M174E/M378E, L648E, L720E, M911E, I18W/A23F/C24F, G575F, and G575K were expressed and purified to greater than 95% homogeneity, as judged by SDS-polyacrylamide gel electrophoresis.

Kinetic Measurements. The rate of glutamine hydrolysis was determined by coupling the formation of glutamate to the production of α-ketoglutarate with L-glutamate dehydrogenase (GDH) and 3-acetylpyridine adenine dinucleotide (APAD).[61] The reaction mixtures contained 50 mM HEPES, pH 7.6, 20 mM $MgCl_2$, 100 mM KCl, 40 mM $KHCO_3$, 5.0 mM ATP, 10 mM ornithine, 1.0 mM APAD, 30 units of GDH, and varying amounts of glutamine. The rate of ADP formation was measured using a pyruvate kinase (PK)/lactate dehydrogenase (LDH) coupling system.[61] The reaction mixtures for the glutamine-dependent assay contained 50 mM HEPES, pH 7.6, 20 mM $MgCl_2$, 100 mM KCl, 40 mM $KHCO_3$, 10 mM glutamine, 10 mM ornithine, 1.0 mM phosphoenolpyruvate, 0.2 mM NADH, 2 units of PK, 3 units of LDH, and varying amounts of ATP. Glutamine was excluded from the HCO_3^--dependent ATPase assays. This assay was followed by monitoring the decrease in absorbance at 340 nm using a Molecular Devices SpectraMax Plus 96-well plate reader. The synthesis of carbamoyl phosphate was determined by measuring the rate of citrulline formation in a coupled assay containing ornithine transcarbamoylase (OTC) and ornithine.[63] The assay mixture contained 50 mM HEPES, pH 7.6, 20 mM $MgCl_2$, 100 mM KCl, 40 mM $KHCO_3$, 5.0 mM ATP, 10 mM ornithine, 12 units of OTC, and 10 mM glutamine. The rate of ATP synthesis was measured with a hexokinase (HK)/glucose-6-phosphate dehydrogenase (G6PDH) coupling system.[61] The assay mixture for the ADP-dependent assay included 50 mM HEPES, pH 7.6, 20 mM $MgCl_2$, 100 mM KCl, 10 mM ornithine, 0.75 mM NAD, 2.0 units HK, 1.0 mM glucose, 1.0 unit G6PDH, 1.0 mM carbamoyl phosphate, and varying amounts of ADP.

Results and Discussion

Water Pockets in the Tunnel. Based on the X-ray crystal structure and MD simulations, the entire carbamate tunnel can be roughly separated into three segments. There are three continuous water-filled pockets connected by two relatively narrow regions near Ala-23 and Gly-575. There are, on average, 21 waters in the first pocket, which extends from the first nucleotide-binding site located in the N-terminal domain of the large subunit to Ala-23. It is worth noting that the water cluster in this region of the tunnel is partly connected to the water surrounding the bound ADP and the external water. As a result, water can exchange between this pocket and the exterior. The middle pocket between Ala-23 and Gly-575 is filled with 9 water molecules, and the last water pocket beyond Gly-575 extends to the ATP-binding site for carbamoyl phosphate synthesis is also filled with 9 water molecules. In contrast to the first water cluster, the latter two pockets are tightly sealed and no exchange of water with the exterior was observed during the simulations. The major difference between the second and third water clusters is that the former is more compact while the latter is more extended in one dimension along the tunnel.

Three individual conventional MD simulations, each generated a 40-ns continuous trajectory, were performed with carbamate positioned in the middle of these three water pockets using complex **A**. The rmsd of the polypeptide backbone along the entire trajectory was computed, and the results (see Figure S2) indicate that the protein is stable during the simulation. A narrow distribution for the position of carbamate was observed in each of the three trajectories as shown in Figure 3. In the first segment of the tunnel, carbamate is localized at a distance of 10 Å (blue curve in Figure 3) and at a position above the center of Glu-25, Glu-383, and Glu-604. In the second segment between Ala-23 and Gly-575, the carbamate distribution centers at a distance of 23 Å (red curve in Figure 3), which is also the center of the water pocket. When carbamate approaches the active site for carbamoyl phosphate synthesis, it is solvated in the third water pocket with a distance distribution that centers at 33 Å. As illustrated in Figure 3, Ala-23 and Gly-575 separate the entire tunnel into three segments, at a distance of 17 and 29 Å, respectively. These conventional MD simulations indicate the existence of well-structured water pockets within the tunnel and the possibility of molecular valves at the narrow parts of the tunnel near Ala-23 or Gly-575 that may control the transport of carbamate.

(60) Javid-Majd, F.; Mullins, L. S.; Raushel, F. M.; Stapleton, M. A. *J. Biol. Chem.* **2000**, *275*, 5073–5080.
(61) Stapleton, M. A.; JavidMajd, F.; Harmon, M. F.; Hanks, B. A.; Grahmann, J. L.; Mullins, L. S.; Raushel, F. M. *Biochemistry* **1996**, *35*, 14352–14361.
(62) Mareya, S. M.; Raushel, F. M. *Biochemistry* **1994**, *33*, 2945–2950.
(63) Snodgras, P. J.; Parry, D. J. *J. Lab. Clin. Med.* **1969**, *73*, 940–950.

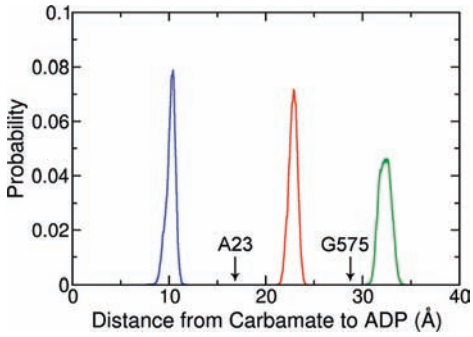

Figure 3. Probability distribution for the position of carbamate in the tunnel. The distance is defined from the carbon atom of carbamate to the β-phosphate of ADP bound at the active site for the carbamate formation. The distributions in the first (near Glu-25, Glu-383, and Glu-604), second (in the middle of the tunnel), and third water pockets (near Glu-577 and Glu-916) are shown in blue, red, and green, respectively.

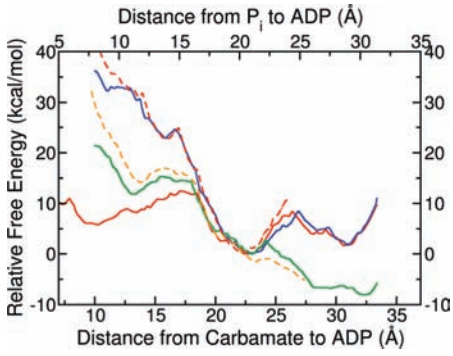

Figure 4. Potentials of mean force from the site of carbamate formation to the site of utilization. The reaction coordinate, labeled on the bottom, is defined as the distance from the carbon atom of carbamate to the β-phosphate of ADP bound at the active site for carbamate formation. The PMFs, with respect to this reaction coordinate, are presented as the solid lines for the complexes **A**, **B**, and **C** in red, blue and green, respectively. The other reaction coordinate, labeled on the top, is defined as the distance from the carbon atom of carbamate to the phosphate product. The PMFs, with respect to the second reaction coordinate, are shown as the dashed curves for the complexes **B** and **C** in red and yellow, respectively.

Potential of Mean Force Along the Entire Carbamate Tunnel. Carbamoyl phosphate is not synthesized until phosphate is released from the active site for carbamate formation and ATP is bound to the active site for the synthesis of carbamoyl phosphate.[64] As a highly charged species, phosphate can induce significant changes in the interactions between carbamate and the protein. Specifically, the side chain of Arg-306, which ion-pairs with the γ-phosphate of ATP or phosphate, is able to rotate toward the tunnel entrance and form hydrogen bonds with Glu-25, Glu-383, and Glu-604 only after phosphate is released from the active site. To better understand the influence of phosphate and the conformational changes of Arg-306, three different complexes were constructed as described earlier and listed in Table 1. The free energy profiles (or PMFs) along the tunnel for the three complexes are shown in Figure 4. The free energy profiles are drastically changed when different combinations of substrates and products are bound in the active site. The three cases are described below.

Complex A: Release of Phosphate. In the absence of bound phosphate, three minima are found at distances of approximately 10, 23, and 31 Å from ADP and two maxima located at 17 and 26 Å (red solid curve in Figure 4). The free energies of the first and third minima, relative to the middle minimum at 23 Å taken as the reference state, are 5.8 and 1.6 kcal/mol, respectively, whereas the two barriers have heights of 6.7 and 8.4 kcal/mol, respectively. In the initial complex prepared for the umbrella sampling calculation, carbamate was positioned in the middle of the tunnel. Within 1-ns relaxation, the side chain of Arg-306 rotates away from the ADP-binding site and forms multiple hydrogen bonds to Glu-25, Glu-383, and Glu-604. Apparently, the release of phosphate into solution frees Arg-306 and the negative charges of the three glutamates attract the side chain of Arg-306. Further umbrella sampling simulations were performed based on this structure with the carbamate positioned at different points along the tunnel.

Complex B: Bound Phosphate and ATP. In the presence of phosphate, the PMF along the first segment of the tunnel is significantly higher compared to complex **A**, whereas the remainder of the trajectory overlaps almost perfectly (blue solid curve in Figure 4). With phosphate present, the interactions within the first portion of the tunnel are much more complicated since this reaction product prevents Arg-306 from rotating toward Glu-25, Glu-383, and Glu-604 by forming strong salt-bridge type hydrogen bonds and thus effectively blocks the migration of carbamate into the tunnel. The very high free energy barrier between 10 and 15 Å is indicative of a strong repulsion between carbamate and the closed gate formed by phosphate and the side chain of Arg-306. Carbamate is thus trapped in the active site. A two-dimensional reaction coordinate was considered necessary to estimate the free energy profile for the penetration of carbamate through the closed gate formed by Arg-306 and phosphate. Carbamate must break one or more hydrogen bonds between Arg-306 and phosphate after passing this gate. In this simulation, the windows on either side of Arg-306 do not have a reasonable connection. The resulting free energy profile near the gate does not converge well, and thus the reaction coordinate starts at 10 Å. Although the free energy barrier for crossing over the gate was unable to be computed using the reaction coordinate and the bias potential applied in this umbrella sampling simulation, the steep free energy profile at distances less than 15 Å demonstrated the impenetrability of the closed gate.

The separation between the first and second water pockets is also observed in this simulation. The sharp peak at 17 Å results from the narrow passage near Ala-23. The negative charges on Glu-25, Glu-383 and Glu-604 also prohibit the entrance of carbamate. However, in complex **A**, the rotation of Arg-306, after the release of phosphate, shields these negative charges from carbamate, thus allowing it to pass through. The free energy profile from 19 to 33 Å is nearly identical to that for complex **A**. Therefore, the conformational change of Arg-306 only affects carbamate transport over short distances.

Complex C: Bound Phosphate and ADP. In this simulation, the side chain of Arg-306 was manually rotated to interact with the side chains of Glu-25, Glu-383, and Glu-604 before the umbrella sampling calculation was initiated. At the active site in the C-terminal domain the side chain of Arg-848 rapidly (less than 1 ns) rotates away from the bound ADP and hydrogen bonds to Glu-577 and Glu-916 in the relaxation run. This conformation was kept for all windows in the umbrella sampling simulation. The free energy profile (green solid curve in Figure 4) is similar to that for case **A** (red solid curve in Figure 4) for the first and second water pockets, especially in the range from

(64) Raushel, F. M.; Anderson, P. M.; Villafranca, J. J. *Biochemistry* **1978**, *17*, 5587–5591.

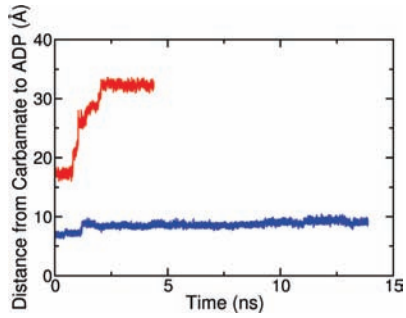

Figure 5. Distance (the first reaction coordinate defined in Figure 4) vs time in the conventional MD simulation for complex **C** (Table 1) started with carbamate in the first water pocket (blue) and near Ala-23 (red).

13 to 23 Å. The steep increase in free energy at distances shorter than 13 Å is a result of strong anion−anion repulsion between phosphate and carbamate. This repulsion also raises the PMF between 13 to 18 Å, relative to the PMF for complex **A** by 1.5−2.5 kcal/mol. However, the free energy profile after the constriction near Ala-23 is overwhelmingly downhill.

The PMF calculated for this case indicates that the transport of carbamate needs to overcome a significant barrier at 15 Å. Once this barrier is passed, the translocation is spontaneous and fast. To test this result, two independent conventional MD simulations were initiated with carbamate positioned in the first water pocket above the glutamine trio and near Ala-23. The results match the free energy profile based on umbrella sampling. Carbamate is translocated more than 15 Å and delivered to the active site for the synthesis of carbamoyl phosphate within 1.6 ns as shown for the successful trajectory in Figure 5 (red curve). On the other hand, carbamate is immobilized in the first water pocket in another trajectory (blue curve). The barrier at 15 Å prevents carbamate from passing into the rest of the tunnel in conventional MD simulations while the downhill potential after the barrier allows the rapid translocation of carbamate to the end of the tunnel.

The two missing loops that span residues 717−723 and 742−749 in the large subunit of CPS (PDB code: 1c3o) indicate that there is considerable flexibility in the γ-phosphate binding region of the protein when ADP, and not ATP, is bound. This flexibility and the smaller size of ADP, relative to ATP, create a larger water pocket. The increased solvation and lack of electrostatic repulsion from the γ-phosphate of ATP stabilize carbamate in the last water pocket. Relative to the middle water pocket, the free energy for carbamate transport into the third water pocket is more stable by 8.2 kcal/mol. More importantly, without the ionic attraction from the γ-phosphate the side chain of Arg-845 is free to rotate and form a hydrogen bond network with Glu-577 and Glu-916. As a consequence, the repulsion from the negative charges on the glutamates are sufficiently shielded by this arginine when carbamate passes through this part of the tunnel, resulting in a significant drop in the barrier between the middle and the last water pocket (red solid curve in Figure 4) although a barrier is still observed at 24 Å with a height of only 1.6 kcal/mol (green solid curve in Figure 4).

The strong repulsion between carbamate and phosphate makes estimation of the PMF difficult when carbamate is close to its site of formation. Thus, the distance between phosphorus (in phosphate) and carbon (in carbamate) was defined as a new reaction coordinate for complexes **B** and **C**. A total of 69 windows were defined with a step size of 0.25 Å and the reaction coordinate ranged from 8.0 to 25.0 Å. The equilibrations were done prior to collecting a continuous 2-ns trajectory for each window. In the equilibration process, the PMF was computed every 500 ps until the PMFs from the last two trajectories virtually overlapped. The PMFs from the second reaction coordinate matched well with the previous ones (red dashed curve vs blue solid curve and yellow dashed curve vs green solid curve in Figure 4).

For complex **B**, the details of the PMF were reproduced by this method as indicated by the two minima for the first and second water pockets and the narrow but sharp barrier at a distance of 15 Å. The free energy increases sharply when carbamate is close to phosphate and the distance is shorter than 10 Å. For complex **C**, the downhill trend of the PMF (yellow dashed curve in Figure 4) is more obvious relative to the previous PMF (green solid curve in Figure 4). Furthermore, the barrier between the second and third water pockets almost disappears at a distance of 22 Å. The very low free energy barrier from the previous calculation is not significant enough to prevent the spontaneous translocation of carbamate through the tunnel. As a result, the simulations based on the second reaction coordinate further confirm that the PMFs calculated on the previous reaction coordinate are reliable for the first and second segments of the tunnel.

The thermodynamic influences of phosphate and the conformational change of Arg-306 can be observed when comparing the PMFs for each of the three systems in the range of 10 to 17 Å (Figure 4). At these positions the PMFs of **A** and **C** are significantly lower than that of **B**, indicating that the rotation of Arg-306 effectively shields the charge−charge repulsion from Glu-25, Glu-383, and Gu-604 with carbamate. The repulsion between phosphate and carbamate results in the PMFs of **B** and **C** to steeply increase when the reaction coordinate is shorter than 13 Å. The PMF segments of **A** and **C** are nearly parallel to each other in the range from 13 to 17 Å, illustrating the structural similarity for these two systems. However, a small difference does exist. The repulsion from phosphate also lifts the PMF of **C** by about 2 kcal/mol, relative to that of **A**.

Conformational Change of Arg-306. The free energy profiles along the tunnel are dramatically affected by the conformational change of Arg-306 as shown in Figure 4 (red and blue solid curves). In order to understand the influence of phosphate on this conformational change, two umbrella sampling simulations were performed with complexes **A** and **B**. The distance between the guanidinium carbon of Arg-306 and the carboxylate carbon of Glu-604 was defined as the reaction coordinate and separated into 20 windows. The side chain of Arg-306 forms hydrogen bonds with Glu-604 when the distance is less than 5 Å (Figure 6b,d) while the side chain points toward ADP when the distance greater than 7 Å (Figure 6a,c). These two conformations are defined as the open and closed forms, respectively. Carbamate was positioned near the β-phosphorus of ADP. In the open form, the passage leading to the tunnel entrance is filled with water while in the closed form the transport of carbamate is blocked by the side chain of Arg-306. Relaxation was performed until equilibrium was reached which was checked by comparing the PMFs for two continuous 500-ps trajectories. The two 500-ps trajectories were followed by a 1-ns trajectory and collected for data analysis. The free energy profiles from the 2-ns umbrella sampling are shown in Figure 7.

After the release of phosphate into solution, carbamate partially fills the void and forms a hydrogen bond with the side chain of Arg-306 (Figure 6a). This hydrogen bond is the major obstacle to the rotation of Arg-306. The overall free energy

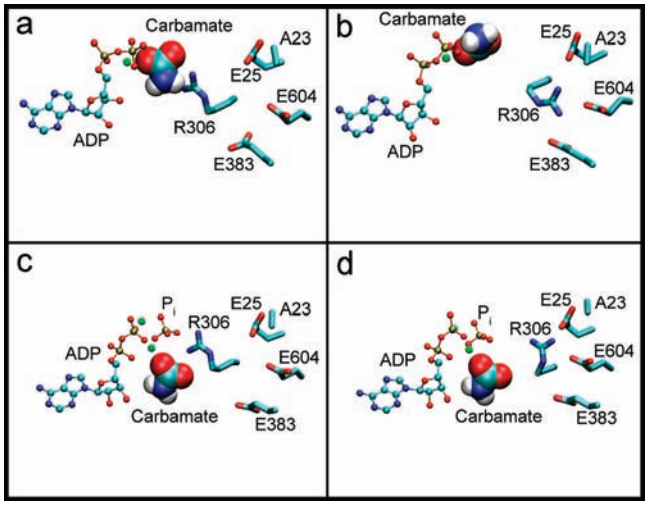

Figure 6. Conformational change of the Arg-306 side chain. In panels A and B, phosphate is released, but in panels C and D, it remains bound. The side chain of Arg-306 orients toward ADP (or phosphate) in panels A and C while it forms a salt bridge with Glu-25, Glu-383, and Glu-604 in panels B and D.

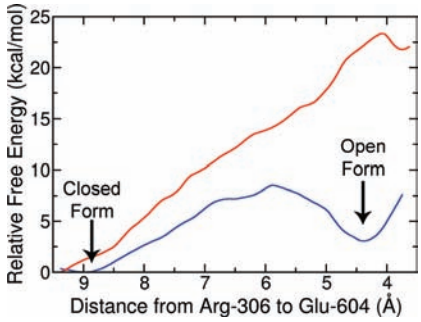

Figure 7. Potentials of mean force for the rotation of the Arg-306 side chain. The reaction coordinate is defined as the distance between the carbon atom in the guanidinium group of Arg-306 and the carbon atom of the side chain carboxylate group of Glu-604. The PMFs for complexes **A** and **B** are plotted as the blue and red curves, respectively.

barrier is 8.0 kcal/mol and the free energy increases by 3.0 kcal/mol after the rotation relative to the closed conformation (blue curve in Figure 7). When phosphate is bound, the electrostatic interactions between phosphate and Arg-306 prohibit this conformational change. As shown in Figure 6d, when Arg-306 forms hydrogen bonds with Glu-25, Glu-383, and Glu-604, the free energy is 22 kcal/mol higher than that for the closed conformation, in which phosphate and Arg-306 bind to one another (red curve in Figure 7), with a barrier of 24 kcal/mol at a distance of 4.1 Å. The conformational change from the closed form to the open form is favored when phosphate is released. Based on transition state theory, the barrier height of 24 kcal/mol corresponds to a reaction rate of approximately one turnover every few hours. This rate is more than a thousand fold slower than the synthesis of carbamoyl phosphate.

In conventional MD simulations for complexes **A** and **B** with carbamate positioned in the middle water pocket as initial geometries, the rotation of Arg-306 occurs in less than 1 ns in complex A while the hydrogen bonds are kept between phosphate and Arg-306 in a 18-ns trajectory in complex **B** with bound phosphate. The conformational change of Arg-306 is almost barrierless if carbamate does not directly interact with the guanidino group of the arginine. A free energy barrier of 8.0 kcal/mol is not prohibitively high and the corresponding conformational change is fast enough to protect carbamate from decomposition. These results show that the release of phosphate is critical for the transport of carbamate. The conformational change of Arg-306 opens the tunnel for the entry of carbamate into the tunnel and also shields charge−charge repulsion from Glu-25, Glu-308, and Glu-604.

The conformational change of Arg-848 was also observed when ADP is bound at the site for carbamoyl phosphate synthesis in complex **C**. By shielding the repulsion from Glu-577 and Glu-916, the relative free energy for carbamate translocation in the last water pocket is significantly lowered (green solid curve vs red solid curve in Figure 4). However, this preference does not lead to a productive overall synthesis since ATP is not available near the tunnel exit. A direct comparison between Arg-306 and Arg-848 is not very meaningful because the hydrogen bonds between phosphate and Arg-306 isolates carbamate from the tunnel while similar interactions between ATP and Arg-848 are not capable of prohibiting the reaction between carbamate and the γ-phosphate of ATP. The conformational change of Arg-848 may be related to the release of carbamoyl phosphate and/or ADP from this active site.

Rates of Carbamate Transfer. To estimate the transfer rates of carbamate through the two narrow segments of the tunnel near Ala-23 and Gly-575, Kramers' reaction rate theory was used. Assuming that the dynamics can be described by a one-dimensional diffusion along the reaction coordinate in which both the reactant well and the barrier top are parabolic, the rates in complex environments can be computed using eq 1.[65−67] In eq 1, ω_{min} and ω_{max} are frequencies that characterize the curvature of the free energy profile at the minimum and barrier top, respectively, k_B is Boltzmann's constant, T is the absolute temperature, h is Planck's constant, ΔG^* is the height of the free energy barrier, R is universal gas constant, and D_{min} and D_{max} are the diffusion constants at the minimum and barrier top, respectively, shown in Figure 3. D_{min} for carbamate and ω_{min} were fit to 0.00673 Å^2/ps and 0.478 s^{-1} for the first barrier of 6.7 kcal/mol at 17.2 Å, whereas they were fit to 0.00338 Å^2/ps and 1.278 s^{-1} for the second barrier of 8.4 kcal/mol at 26.4 Å (red solid curve in Figure 4). Thus, from eq 1, $\tau = 123.2$ and 629.4 μs, respectively. It takes ~0.6 ms for carbamate to be delivered from the middle pocket to the end of the tunnel by overcoming the highest free energy barrier imposed by the narrow segment near Ala-23. This rate-determining step results in a rate constant of 1600 s^{-1}, which is ~440-fold faster than the rate constant for the overall synthesis of carbamoyl phosphate. Therefore, the barrier for the transport of carbamate through the tunnel is too low for it to be the rate-determining step for this enzyme.

$$\tau = \frac{2\pi k_B T}{\omega_{min}\omega_{max}D_{max}} \exp\left(\frac{\Delta G^*}{RT}\right) \approx \frac{2\pi k_B T}{\omega_{min}{}^2 D_{min}} \exp\left(\frac{\Delta G^*}{RT}\right) \quad (1)$$

Electrostatic Potential of the Tunnel Wall Surface. The electrostatic potential and corresponding charge distribution on the tunnel wall surface were computed using AMBER's MM_PBSA (molecular mechanics-Poisson−Boltzmann/surface

(65) Kramers, H. A. *Physica* **1940**, *7*, 284–304.
(66) Berne, B. J.; Borkovec, M.; Straub, J. E. *J. Phys. Chem.* **1988**, *92*, 3711–3725.
(67) Socci, N. D.; Onuchic, J. N.; Wolynes, P. G. *J. Chem. Phys.* **1996**, *104*, 5860–5868.

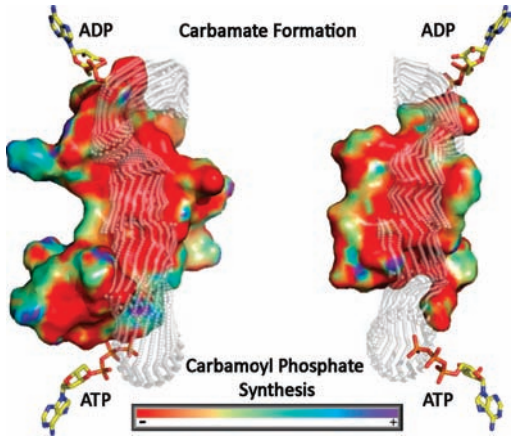

Figure 8. Electrostatic potential on the tunnel wall surface. The tunnel is shown in transparent beads and tunnel wall is shown in two halves. The carbamate formation site is positioned on the top of this figure with ADP bound while the carbamoyl phosphate synthesis site is on the bottom with ATP bound.

area) module.[68] As shown in Figure 8, the surrounding wall is largely negatively charged. With a negatively charged environment, carbamate is able to travel quickly through the tunnel with few interactions with residues in the tunnel. In addition, the end of the tunnel appears to have a higher electrostatic potential than the beginning, consistent with the direction of the transport of the negatively charged carbamate.

Selection of Mutation Sites. Amino acid residues within the carbamate tunnel were mutated in an attempt to engineer blockages that would impede the migration of carbamate from one active site to the next. A triple mutant, I18W/A23F/C24F, was initially constructed to fill the large water cluster in the middle pocket of the tunnel and impede the translocation of carbamate. Ala-23 was mutated previously to leucine and tryptophan to create a barrier inside the tunnel.[69] The kinetic constants of the A23W mutant indicated that a structural perturbation of the active site for the synthesis of carbamate had occurred. Since the original goal of this experiment was to hinder the migration of carbamate through the tunnel rather than disrupt the rate of carbamate formation, it was anticipated that an A23F mutation may be sufficient to accomplish this task without unwanted structural effects on the catalytic centers. The analogous mutant, G575F, was constructed at the opposite end of the carbamate tunnel. Previously, Gly-575 was mutated to alanine, serine, and leucine in an effort to probe the size of the tunnel in this region of the protein.[4,69] These substitutions to Gly-575 did not exhibit significant perturbations to the kinetic constants for the partial reactions. However, the G575L mutant had a 50-fold reduction in the rate of carbamoyl phosphate formation. This was attributed to the restricted passage of carbamate through the tunnel. The insertion of a larger phenylalanine side chain was anticipated to create a more efficient blockage of the tunnel. Two additional mutants, A23K and G575K, were made to affect the conformational orientation of Arg-306 and Arg-848 by competing for ionic interactions with Glu-25, Glu-383, Glu-577, Glu-604, and Glu-916.

Further attempts to disrupt putative interactions between the two special arginine residues (Arg-306 and Arg-848) and the five interior glutamate residues prompted the construction of mutants M174E, M378E, and M174E/M378E. Met-174 and Met-378 are reasonably close to Arg-306 and are on the opposite face of the tunnel wall near the first triad of glutamate residues. If Arg-306 were to interact with either of these new glutamate residues, the tunnel may remain in a more open conformation. The analogous pair of residues, Met-911 and Leu-720, were chosen at the other end of the carbamate tunnel near the active site for the synthesis of carbamoyl phosphate. Leu-648 was mutated to a glutamate to facilitate the formation of a salt bridge between this residue and Arg-845. The formation of salt bridges within the tunnel would block the exit of the carbamate tunnel, preventing carbamate from reaching the second molecule of ATP bound at the carbamoyl phosphate active site.

Kinetic Properties of Carbamate Tunnel Mutants. The triple mutant, I18W/A23F/C24F, was made to disrupt the water pocket that may facilitate the passage of carbamate through the carbamate tunnel. While this mutant significantly hindered the overall rate of carbamoyl phosphate synthesis, it also diminished all of the other partial reactions. Therefore, substitution of three very large residues for three smaller residues may have caused unwanted conformational changes inside the protein, and perturbed the conformation of the two active sites. To diminish this problem, a single mutation, A23F, was constructed and characterized. The methyl side chain of Ala-23 points directly into the interior of the carbamate tunnel and thus the substitution with phenylalanine may be sufficient to block this part of the tunnel. From the kinetic data the only reaction significantly affected by this mutation was the overall synthesis of carbamoyl phosphate (Tables 2 and 3). A similar kinetic pattern was observed for the analogous mutation (G575F) near the active site for the synthesis of carbamoyl phosphate. This mutant has wild-type-like activity in all of the partial reactions except for the carbamoyl phosphate synthesis reaction. Of the mutants made in the carbamate tunnel, G575F is the most efficacious at blocking the passage of carbamate without disrupting any of the active sites.

The substitution of Ala-23 with lysine decreased the glutamine-dependent ATPase activity by an order of magnitude. While there was a decrease in the rate of carbamoyl phosphate formation, the enzyme utilized two molecules of ATP for every molecule of carbamoyl phosphate synthesized. The analogous mutant, G575K, at the other end of the carbamate tunnel, had similar catalytic properties as the wild-type protein, suggesting that the conformational change of Arg-848 may not be crucial for the transport of carbamate.

The single mutants, M174E and M378E, which were created to form a salt bridge with Arg-306, were successful in disrupting the passage of carbamate through the tunnel. These mutants had significant reductions in the rates of the ATPase and carbamoyl phosphate synthesis reactions. Neither mutation affected the rate of the partial ATP synthesis reaction (Tables 2 and 3). The catalytic properties of the double mutant, M174E/M378E, are similar to the single mutants with regard to the various partial reactions. However, the double mutant was unable to synthesize carbamoyl phosphate.

The mutant L648E was successful at diminishing the synthesis of carbamoyl phosphate but the mechanism may be different from a simple blockage of the tunnel. The formation of a salt bridge between this glutamate and Arg-845 cannot block the exit of the tunnel but it can potentially interfere with the reaction between carbamate and ATP. There was no detectable rate of carbamoyl phosphate formation. Little effect on the rates of all partial reactions was observed. Thus the reactions at the small subunit and the carboxy phosphate active sites remained

(68) Luo, R.; David, L.; Gilson, M. K. *J. Comput. Chem.* **2002**, *23*, 1244–1253.
(69) Kim, J.; Howell, S.; Huang, X. Y.; Raushel, F. M. *Biochemistry* **2002**, *41*, 12575–12581.

Table 2. Kinetic Characterization of the Wild-Type and Mutant Forms of CPS

	Gln-dependent ATPase		HCO_3^--dependent ATPase[a]		glutaminase	
enzyme	k_{cat} (s^{-1})	K_m (mM ATP)	k_{cat} (s^{-1})	K_m (mM ATP)	k_{cat} (s^{-1})	K_m (mM Gln)
wild type	3.60 ± 0.11	0.24 ± 0.04	0.170 ± 0.003	0.051 ± 0.008	2.20 ± 0.04	0.15 ± 0.01
I18W/A23F/C24F	0.06 ± 0.002	0.25 ± 0.05	0.039 ± 0.002	0.21 ± 0.05	0.13 ± 0.01	0.16 ± 0.04
A23F	1.30 ± 0.07	1.60 ± 0.25	0.097 ± 0.005	0.12 ± 0.04	1.08 ± 0.04	0.21 ± 0.03
A23K	0.28 ± 0.01	0.38 ± 0.08	0.17 ± 0.01	0.33 ± 0.06	0.21 ± 0.02	0.10 ± 0.04
G575F	3.30 ± 0.19	0.014 ± 0.030	0.19 ± 0.01	0.014 ± 0.003	3.00 ± 0.14	0.19 ± 0.03
G575K	3.3 ± 0.18	0.070 ± 0.01	0.18 ± 0.01	0.013 ± 0.002	3.10 ± 0.20	0.17 ± 0.04
M174E	0.11 ± 0.01	0.69 ± 0.17	0.053 ± 0.002	0.36 ± 0.05	0.15 ± 0.01	0.39 ± 0.06
M378E	0.035 ± 0.002	0.160 ± 0.04	0.013 ± 0.008	0.030 ± 0.008	0.13 ± 0.01	0.35 ± 0.07
M174E/M378E	0.043 ± 0.002	0.28 ± 0.07	0.028 ± 0.001	0.29 ± 0.07	0.10 ± 0.01	0.47 ± 0.11
L648E	3.2 ± 0.20	1.2 ± 0.22	0.59 ± 0.03	0.50 ± 0.09	1.3 ± 0.1	0.23 ± 0.03
L720E	2.0 ± 0.15	1.7 ± 0.36	0.39 ± 0.01	0.22 ± 0.03	0.84 ± 0.03	0.18 ± 0.02
M911E	0.50 ± 0.05	1.0 ± 0.31	0.33 ± 0.01	0.26 ± 0.04	0.14 ± 0.01	0.18 ± 0.05

[a] HCO_3^--dependent ATPase activity was measured in the absence of glutamine.

Table 3. Kinetic Characterization of ATP and Carbamoyl Phosphate (CP) Synthesis Activities

	ATP synthesis[a]		CP synthesis	
enzyme	k_{cat} (s^{-1})	K_m (mM ADP)	k_{cat} (s^{-1})	ATP:CP
wild type	0.130 ± 0.005	0.13 ± 0.03	1.90 ± 0.01	1.9
I18W/A23F/C24F	0.086 ± 0.003	0.18 ± 0.03	<0.01	
A23F	0.230 ± 0.004	0.53 ± 0.007	0.033 ± 0.004	39
A23K	0.32 ± 0.01	0.022 ± 0.006	0.160 ± 0.002	1.8
G575F	0.058 ± 0.002	0.030 ± 0.005	0.072 ± 0.001	46
G575K	0.15 ± 0.007	0.054 ± 0.01	1.9 ± 0.01	1.8
M174E	0.10 ± 0.002	0.088 ± 0.01	1.90 ± 0.01	1.8
M378E	0.20 ± 0.004	0.13 ± 0.01	0.012 ± 0.002	2.9
M174E/M378E	0.22 ± 0.005	0.17 ± 0.02	<0.01	
L648E	0.024 ± 0.0004	0.34 ± 0.03	<0.01	
L720E	0.031 ± 0.001	0.42 ± 0.078	<0.01	
M911E	<0.01		0.015 ± 0.0004	33.3

[a] From ADP and carbamoyl phosphate.

unperturbed. The L648E mutant exhibited a 10-fold drop in the rate of the glutaminase reaction which is due to the uncoupling between the carboxy phosphate and glutaminase active sites (Tables 2 and 3).

The residues analogous to Met-174 and Met-378, Leu-720 and Met-911, respectively, were mutated to glutamate. The rates for both the glutamine- and HCO_3^--dependent ATPase reactions were largely unaffected by these mutations. The rate of the partial ATP-synthesis reaction was decreased 4-fold for the L720E mutant and virtually undetectable for the M911E mutant. These perturbations may be due to an altered active site environment which diminishes the rate ADP phosphorylation by carbamoyl phosphate. No carbamoyl phosphate formation was detected with the L720E mutant while only limited formation was detected with M911E (Table 3). Both mutants can structurally block the exit of the carbamate tunnel although the presence of these glutamates also weakens the assistance of Arg-848 during the synthesis of carbamoyl phosphate.

Summary

The existence of an intramolecular tunnel for the transport of carbamate within the large subunit of carbamoyl phosphate synthetase was supported by molecular dynamics simulations. Conventional MD simulations for each section of the nearly 40 Å tunnel were performed and indicate that the passageway is tightly sealed since no leakage of carbamate was observed. The calculations also show that the release of phosphate is necessary and the free energy profile along the tunnel is largely downhill without prohibitively high barriers. The release of phosphate allows the side chain of Arg-306 to rotate toward the entrance of the tunnel and form strong hydrogen bonds with Glu-25, Glu-383, and Glu-604. This conformational change opens the entrance to the tunnel and shields charge−charge repulsion from the three glutamates to carbamate when this intermediate passes through this segment of the tunnel. When phosphate is bound, the rotation of the arginine side chain is prohibited by a free energy barrier with a height of at least 23.4 kcal/mol. The importance of Arg-306 and the trio of glutamate residues within the tunnel is confirmed by the fact that neither of the mutants, R306A nor E25Q/E383Q/E604Q, are able to synthesize carbamoyl phosphate.[70]

The transfer of carbamate through the tunnel is rapid with two free energy barriers of 6.7 and 8.4 kcal/mol at the narrow parts near Ala-23 and Gly-575, respectively. Three water pockets were located at the entrance, the middle and the exit of the tunnel, filled with 21, 9, and 9 waters, respectively, and the corresponding relative free energies are 5.8, 0, and 1.6 kcal/mol. The free energy profiles along the tunnel change dramatically when different nucleotides are bound. A successful transfer of carbamate through the middle and last water pockets was observed in a conventional MD trajectory when ADP, instead of ATP, is bound to the active site for carbamoyl phosphate synthesis. Based on these simulations, two mutants, A23F and G575F, were designed to block or impede the migration of carbamate through the two narrow portions of the tunnel. The mutants retained less than 4% of the overall activity for the synthesis of carbamoyl phosphate relative to the wild type CPS, while the activities for the ATPase and glutaminase reactions were not damaged.

Acknowledgment. This work was supported in part by the Robert A. Welch Foundation (A-840 to F.M.R. and A-1628 to Y.Q.G.) and the NIH (DK-030343 to F.M.R.). The supercomputer facilities, BRAZOS and HYDRA, at Texas A&M University were deeply appreciated. The SGI Altix 3-node cluster, MEDUSA, at the Department of Chemistry was supported by the NSF (NSF-DMS 0216275). Y.Q.G. is a 2006 Searle Scholar and a 2009 Changjiang Scholar.

Supporting Information Available: The complete author lists for refs 46 and 47 are provided. The PMFs for two different reaction coordinates and the rmsd vs time for the backbone of the large subunit backbone are provided in Figures S1 and S2. Also included is a short movie that shows the movement of carbamate from the site of formation to the site of utilization in the large subunit. This material is available free of charge via the Internet at http://pubs.acs.org.

JA910441V

(70) Kim, J.; Raushel, F. M. *Arch. Biochem. Biophys.* **2004**, *425*, 33–41.